

**Special Section:**

Forum for Arctic Modeling and  
Observational Synthesis (FAMOS)  
2: Beaufort Gyre Phenomenon

**Key Points:**

- Passive tracer reveals Pacific Water mainly circulates along the transpolar route in the Arctic Ocean
- Model resolution plays a big role in simulating liquid freshwater storage within Beaufort Gyre
- Difference in simulated Beaufort Gyre freshwater content is caused by the lateral advection processes

**Supporting Information:**

- Supporting Information S1
- Figure S1
- Figure S2
- Figure S3
- Figure S4
- Figure S5a
- Figure S5b
- Figure S6
- Figure S7
- Figure S8
- Figure S9
- Figure S10
- Figure S11

**Correspondence to:**

P. G. Myers,  
pmyers@ualberta.ca

**Citation:**

Hu, X., Myers, P. G., & Lu, Y. (2019). Pacific Water pathway in the Arctic Ocean and Beaufort Gyre in two simulations with different horizontal resolutions. *Journal of Geophysical Research: Oceans*, 124, 6414–6432. <https://doi.org/10.1029/2019JC015111>



Received 28 FEB 2019

Accepted 11 AUG 2019

Accepted article online 15 AUG 2019

Published online 31 AUG 2019

## Pacific Water Pathway in the Arctic Ocean and Beaufort Gyre in Two Simulations With Different Horizontal Resolutions

Xianmin Hu<sup>1,2</sup> , Paul G. Myers<sup>1</sup> , and Youyu Lu<sup>2</sup>

<sup>1</sup>Department of Earth and Atmospheric Sciences, University of Alberta, Edmonton, Alberta, Canada, <sup>2</sup>Ocean and Ecosystem Sciences Division, Bedford Institute of Oceanography, Fisheries and Oceans Canada, Dartmouth, Nova Scotia, Canada

**Abstract** A set of numerical simulations (with horizontal resolutions of 1/4° and 1/12°) is conducted to study the Pacific Water pathway in the Arctic Ocean and the freshwater content in Beaufort Gyre. Passive tracer tags the Pacific Water entering through Bering Strait into the Arctic Ocean and further reveals its circulation routes and spatial distribution. Both the 1/4° and 1/12° simulations show Pacific Water mainly follows the Transpolar Drift over the integration period of 2002–2016, with a limited amount being able to flow eastward along the Alaskan coast to enter the Canadian Arctic Archipelago. However, the circulation pattern of Pacific Water within the Beaufort Gyre is quite different with a stronger and tighter anticyclonic circulation in the 1/12° simulation corresponding to the difference in freshwater content. The 1/12° simulation successfully reproduces the overall recent increasing trend in the freshwater content in the Beaufort Gyre, while the 1/4° simulation fails to maintain the high freshwater content state after 2007. Budget analysis suggests that this difference in Beaufort Gyre freshwater storage is mainly caused by lateral advection. The lateral freshwater flux is decomposed into two components due to the slow-varying circulation and mesoscale eddies. The difference in the capability to resolve eddies in the two simulations causes the difference in the temporal evolution of both components of the lateral flux.

### 1. Introduction

The Arctic Ocean has a small and generally deep basin, with broad shelves and surrounded mainly by land, with limited connections to the rest of the world ocean (Figure 1). The only connection to the Pacific Ocean is through the narrow and shallow Bering Strait. Multiyear sea ice was observed flowing south through Bering Strait out of the Arctic Ocean during the winter of 2011–2012 (Babb et al., 2013), and Woodgate et al. (2005) observed flow to the south under northerly winds. However, in general, the flow through Bering Strait is to the north, into the Arctic Ocean, driven by the meridional sea level gradient (Coachman & Aagaard, 1966; Aagaard et al., 2006). This inflow has been observed since 1990 by a year-round mooring array (Woodgate, 2018). Historical measurements pointed to a mean inflow of 0.8 Sv (Woodgate & Aagaard, 2005; Woodgate et al., 2005, 2006), although more recent observations show a long-term increase of 0.01 Sv/year, leading to an observed maximum of 1.2 Sv in 2014 (Woodgate, 2018). These same observations also indicate significant seasonal and interannual variability (Woodgate, 2018). The increasing strength of the inflow has also led to increases in the heat and freshwater transports into the Arctic Ocean, with these fluxes reaching maxima of  $5.5 \times 10^{20}$  J and  $\sim 3,500$  km<sup>3</sup> in 2014 (Woodgate, 2018). Thus, Pacific Water (PW) plays a major role in setting and defining the structure of the halocline, especially in the Canada Basin (Bauch et al., 1995; Woodgate & Aagaard, 2005) as well as being the second largest source of freshwater to the Arctic Ocean (Carmack et al., 2016). The heat inflowing with the PW may trigger seasonal sea ice melt (Serreze et al., 2016; Shimada et al., 2006; Woodgate et al., 2006, 2010) as well as playing a role in the recent loss of sea ice in the western Arctic (e.g., Brugler et al., 2014). The PW is also rich in nutrients and thus important to the ecosystems and productivity along the western Arctic shelf (Coachman et al., 1975; Grebmeier et al., 2006; Tsubouchi et al., 2013), but also leads to acidification (Cross et al., 2018).

PW first enters the Arctic in the Chukchi Sea, where it generally follows three main flow branches (Spall et al., 2018). There is more uncertainty about how PW then gets off the shelf. Most studies indicate that important pathways of this export are through Herald Canyon, Central Channel, and Alaskan Coast,

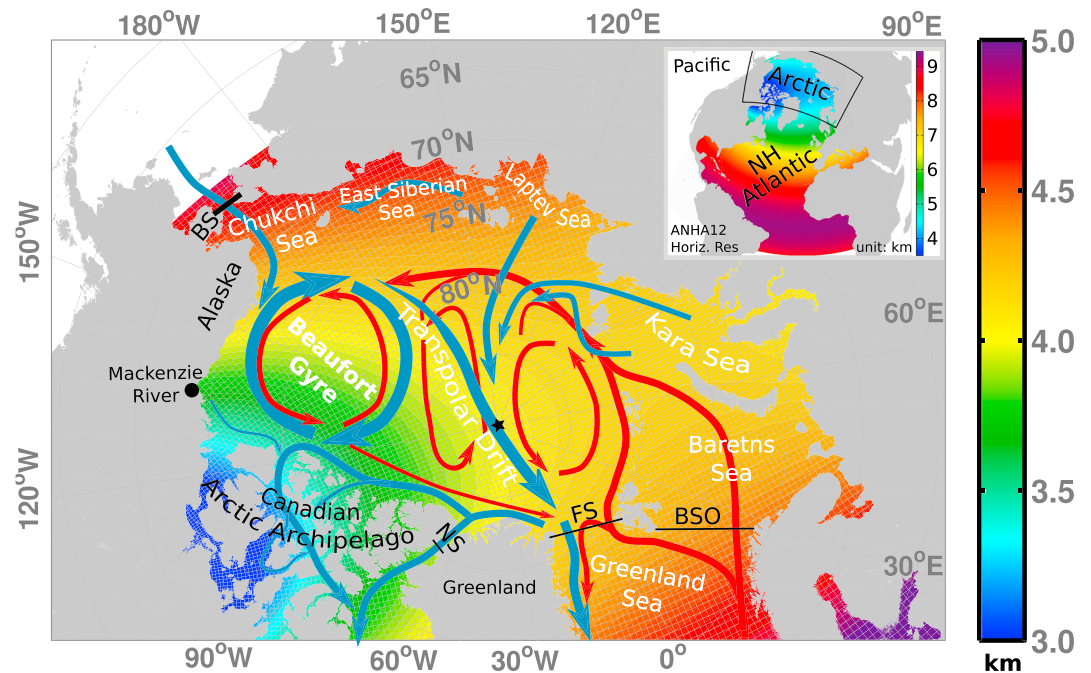


**Figure 1.** ANHA12 mesh grid (every tenth grid point) and horizontal resolution (colors, unit: kilometers) in the Arctic region (thick black box highlighted in the ANHA12 domain shown in inset with a different color scale for the horizontal resolution). Arrows show the schematic ocean circulation (light blue: Pacific inflow and Arctic Ocean surface circulation; red: inflow and circulation of Atlantic Water). The black straight lines show the main gateways (BS = Bering Strait; NS = Nares Strait; FS = Fram Strait; BSO = Barents Sea Opening). The black star represents the location of the North Pole. AHNA = Arctic Ocean and the Northern Hemisphere Atlantic.

although the relative importance of each route is still up for debate (Brugler et al., 2014; Gong & Pickart, 2015; Itoh et al., 2012, 2013; Pickart et al., 2016; Spall et al., 2018; Weingartner et al., 2017; Woodgate & Aagaard, 2005). It has also been suggested that there is exchange of PW directly across the Chukchi shelf break by either wind-driven or eddy processes (Timmermans et al., 2017) although a modeling study by Spall et al. (2008) suggested that the eddies only fluxed tracer, but not mass, across the shelf. A complication may be that Mizobata et al. (2016) suggested from a tracer experiment that the pathway of PW offshore can be altered by changes in the shape and structure of the Beaufort Gyre (BG). That said, a more recent study using a high-resolution numerical model suggests that advection through Barrow Canyon dominates and is the main source of PW to the offshore Canada Basin (Spall et al., 2018).

Many of the studies of PW pathways within the Arctic Ocean have used chemical tracers (e.g., Broecker et al., 1998; Jones & Anderson, 1986) and nutrients. Jones et al. (1998) showed that the ratio of nitrate to phosphate could distinguish Pacific versus Atlantic origin waters. Using this approach, it was shown that PW was the major source of freshwater to the Canada Basin (Carmack et al., 2008; Jones et al., 2008; Yamamoto-Kawai et al., 2008). Additionally, Jones et al. (1998) found two pathways of PW from the Chukchi Plateau: (1) a coastal branch flowing eastward along the Alaskan coast to feed into the Canadian Arctic Archipelago (CAA) and (2) a central Arctic branch entering the deep basin along the Mendeleev Ridge, recirculating in the Canada and Makarov Basins before being transported in the Transpolar Drift toward the north of Greenland and Fram Strait. Jones et al. (2008) showed that much of the deeper PW followed the second route. Steele et al. (2004) discussed these two pathways for PW and pointed that both pathways were observed when the Arctic Oscillation index is high, while the majority of the PW is entrained into the BG when the Arctic Oscillation index is low. Meanwhile, Alkire et al. (2007) suggested that interannual variability in the position of the Transpolar Drift controlled variations in PW in the central Arctic. Lique et al. (2010), using a Lagrangian analysis based on a numerical model, found similar patterns to Steele et al. (2004) but with most of PW leaving the Arctic via the CAA. Yet PW has been detected in multiple studies in Fram Strait (e.g., Alkire et al., 2010; Dodd et al., 2009, 2012).

Aksenov et al. (2016) investigated PW pathways using a suite of numerical models, as part of a Forum for Arctic Modelling and Observational Synthesis coordinated experiment. They suggested links between the pathways out of the Chukchi Sea and the resulting fate of PW. This includes Barrow Canyon feeding the Alaskan shelf, CAA and the Baffin Bay and Herald Canyon water feeding the Transpolar Drift and eventually Fram Strait, while water from the central Chukchi Sea fed the BG. They also suggested that the winds, through Ekman pumping, drives the seasonal and interannual variability of these pathways.

The largest freshwater storage in the Arctic Ocean is within the BG, which is a function of strong Ekman pumping associated with the Arctic high (Proshutinsky et al., 2009). The same paper (Proshutinsky et al., 2009) documents a significant change in freshwater content (FWC) in the 1990s associated with an atmospheric regime shift, leading to a strong positive trend in freshwater over 2003–2007. The increase was part of an overall Arctic Ocean increase of freshwater of  $600 \pm 300 \text{ km}^3/\text{year}$  between 1992 and 2012 (Rabe et al., 2014), with largest increases in the Canada Basin and BG (Rabe et al., 2011). Despite this increase, the meteoric water content of the Arctic Ocean was in a near balance over 2003–2008 (Alkire et al., 2017). The increases in the BG were associated with shifts in freshwater pathways and a decrease in the FWC of the Eurasian Basin (Morison et al., 2012). Wang et al. (2018) pointed out that Arctic sea ice decline significantly contributed to the BG reaching its presently unprecedented levels of FWC. Using satellite radar altimetry and Gravity Recovery and Climate Experiment data, Armitage et al. (2016) showed a doming of dynamic ocean topography in the Beaufort Sea, with a concurrent increase in sea surface height (SSH) and freshwater. Armitage et al. (2017) found an increase in geostrophic currents over the same period, especially in summer. In particular, Armitage et al. (2017) observed a more than doubling of the northwestward current in the southwest BG, linked to a shifting of the circulation of the gyre to the northwest. Regan et al. (2019) used the SSH fields developed by Armitage et al. (2016, 2017) to show that the gyre expanded to the northwest, approaching the Chukchi Plateau and Mendeleev Ridge between 2003 and 2014, with the gyre strength responding to the atmospheric forcing, although Zhang et al. (2016) suggested that the BG has stabilized since 2008, including a leveling of SSH.

Yang et al. (2016) examined the dynamics of the BG using a nonlinear wind-driven two-layer model, showing that the BG differs from lower latitude gyres because of the small size of  $\beta$  and the absence of a western boundary (although subsurface topography may partially substitute for this boundary). Additionally, Yang et al. (2016) showed that the main balance of the time mean circulation is between the curl of the wind stress and eddy fluxes. Both Manucharyan and Spall (2016) and Meneghello et al. (2017) showed that mesoscale eddies control variations in FWC by opposing the tendency of the Ekman pumping to deepen the halocline. Based on ice-tethered profiler data, Zhao et al. (2016) showed that the greatest numbers of eddies were along the south and western boundaries of the BG, with the number of lower halocline eddies reaching a maximum in 2013–2014. Manucharyan et al. (2016) developed a theory for the BG, showing that mesoscale eddy diffusivity controls gyre stability. Thus, on interannual and longer time scale, Ekman pumping and eddy fluxes equally control variations in FWC (Manucharyan et al., 2016), but with significant changes in the FWC only possible through significant changes in the Ekman pumping.

Hu and Myers (2013) presented two major routes for PW to transit and then exit the Arctic Ocean, via the Transpolar Drift and Fram Strait, or through the CAA. They then suggested that when the BG was strong and deep, the water that entered the CAA came from the Transpolar Drift, but during periods with a weakened BG, PW was able to follow the Alaskan Shelf to the CAA. In other words, Hu and Myers (2013) stated that the spatial distribution of the freshwater within the Canada Basin sets the pathways for PW. However, it could be argued that the study of Hu and Myers (2013) has several major limitations. These include the following: (1) It was based on a relatively coarse resolution  $1/4^\circ$  simulation; (2) monthly model velocity fields were used for off-line Lagrangian particle tracking, which involves temporal interpolation and subgrid-scale processes (i.e., mixing and diffusion) not included in the Lagrangian tracking process; (3) forcing was based on climatology, assuming each freshwater state can last 10 or more years without any interannual variability. Thus, it was more an idealized study. Thus, we wish to go back and reexamine the analysis of Hu and Myers (2013) in a more realistic study. A reexamination also makes sense in the context that in recent years, FWC in the Beaufort Sea has been increasing (e.g., Proshutinsky et al., 2009). This provides a perfect opportunity to study PW pathway in a high FWC situation including the interannual variability.

This paper starts with a brief description of the simulation set (horizontal resolution of  $1/4^\circ$  and  $1/12^\circ$ , respectively) and passive tracer design in the next section. In section 3, first, the PW pathway revealed by pas-

sive tracer is presented and the difference in the simulated pathway is related to the difference in FWC. Then, we focus on the simulated FWC time series in the BG as well as a budget analysis from the 1/12° simulation. After that, the causes of BG FWC differences between the two simulations are investigated. A summary and discussion are given in section 4.

## 2. Methods

### 2.1. Numerical Model Description

In this study, the coupled ocean and sea ice system is based on the Nucleus for European Modeling of the Ocean (available at <https://www.nemo-ocean.eu>) Version 3.4 (Madec & the NEMO team, 2008). The sea ice module used here is the Louvain-la-Neuve sea Ice Model Version 2 with an elastic-viscous-plastic rheology (Hunke & Dukowicz, 1997), including both thermodynamic and dynamic components (Bouillon et al., 2009; Carmack et al., 2008; Fichefet & Maqueda, 1997).

The entire model domain covers the Arctic Ocean and the Northern Hemisphere Atlantic (ANHA) with two open boundaries, one close to Bering Strait in the Pacific Ocean and the other one at 20° S across the Atlantic Ocean (Figure 1, inset). Model grids with two horizontal resolutions are set up: One is nominal 1/4° in longitude/latitude (hereafter ANHA4), and the other one is 1/12° (hereafter ANHA12), which are extracted from the corresponding global tripolar ORCA (Madec & Imbard, 1996) grids, ORCA025 and ORCA12, respectively, created by the Drakkar Group (2007). Benefiting from the tripolar grid, ANHA12 has a horizontal grid spacing of less than 4.5 km in most regions in the Arctic Ocean (Figure 1), while it is ~12 km in ANHA4. In the vertical, there are 50 geopotential levels with higher resolution focused on the upper ocean. Layer thickness smoothly transitions from ~1 m at the surface (22 levels for the top 100 m) to 458 m at the last level. Partial steps (Barnier et al., 2006) are enabled to better resolve the seafloor.

In the ocean module, (1) the vector form energy-entropy conserving scheme is used for the horizontal momentum advection. Momentum lateral diffusion is calculated by the bi-Laplacian formulation with the maximum horizontal eddy viscosity set to  $-1.0 \times 10^{10} \text{ m}^4/\text{s}$  and  $-1.0 \times 10^{11} \text{ m}^4/\text{s}$  for ANHA12 and ANHA4, respectively. In space, the horizontal viscosity varies proportionally to the cube of the grid size; (2) the total variation dissipation scheme (Lévy et al., 2001) is used for the horizontal tracer advection. Tracer lateral diffusivity is based on an iso-neutral Laplacian operator. The horizontal tracer diffusivity is proportional to the grid size with an upper limit of  $50.0 \text{ m}^2/\text{s}$  for ANHA12 and  $300.0 \text{ m}^2/\text{s}$  for ANHA4; (3) 1.5-order turbulent kinetic energy closure scheme is used for vertical mixing with the background turbulent kinetic energy set to  $1 \times 10^{-6} \text{ m}^2/\text{s}^2$ . The background vertical eddy viscosity and diffusivity are set to  $1 \times 10^{-4} \text{ m}^2/\text{s}$  and  $1 \times 10^{-5} \text{ m}^2/\text{s}$ , respectively, for both ANHA4 and ANHA12. Note that the GentMcWilliams parameterization (Gent & McWilliams, 1990) is not used in either simulation. The model time step is 180 s for ANHA12 and 1,080 s for ANHA4.

The simulations are integrated from 1 January 2002 to 31 December 2016. Initial conditions, including three-dimensional (3-D) ocean fields (temperature, salinity, zonal velocity, and meridional velocity) as well as two-dimensional SSH and sea ice fields (concentration and thickness) are interpolated from the 1/4° GLObal Ocean Reanalysis and Simulations (GLORYS2v3) produced by Mercator Ocean (Masina et al., 2017). GLORYS2v3 product is also used to provide monthly open boundary conditions (temperature, salinity, and horizontal ocean velocities).

To have a more realistic freshwater from the continent into the ocean, the interannual monthly  $1^\circ \times 1^\circ$  river discharge data from Dai et al. (2009) as well as the Greenland meltwater data ( $5 \text{ km} \times 5 \text{ km}$ ) provided by Bamber et al. (2012) were carefully (volume conserved) remapped onto the model grid. The original data sets do not cover the whole study period; that is, Dai et al. (2009) end by 2007, and Bamber et al. (2012) end by 2010. The source data from the last year are repeated for rest years in each simulation. Note that the runoff from Dai et al. (2009) in 2007 is actually the 5-year average values from October 1999 to September 2004. The trend in Greenland meltwater after 2010 is also relatively flat based on the recently updated results from Bamber et al. (2018).

At the surface, the model is driven with high temporal (hourly) and spatial resolution (33 km) atmospheric forcing data from the Canadian Meteorological Centre Global Deterministic Prediction System ReForecasts data set (Smith et al., 2014), including 10-m winds, 2-m air temperature and specific humidity, shortwave and longwave radiation fluxes, and total precipitation. The high-resolution atmospheric forcing data set does



not go back very far from the present day; thus, our simulation is constrained to a relatively short period of January 2002 to December 2016.

No temperature or salinity restoring is enabled in both the simulations used in this study; thus, the model can evolve freely and better represent the physical processes. Model adjustment is not assessed while a previous study using a similar configuration (Roy et al., 2015) suggested that the adjustment period is about 3 years for a study focusing on the upper Arctic Ocean. Tides are not included in our simulations; thus, any impact from the tides is not covered in this study.

## 2.2. Passive Tracer Design

To trace PW flowing into the Arctic Ocean, a passive tracer is added along a section across Bering Strait since the beginning of our simulations, that is, 1 January 2002, using the NEMO-TOP module (Aumont et al., 2015). The passive tracer concentration ( $C$ ) is assigned at T points in the Arakawa C grid (Mesinger & Arakawa, 1976) along the selected section and updated every time step with an increment  $\Delta C$  proportional to the volume flux:

$$\Delta C = \frac{v \cdot e1v \cdot e3v}{e1t \cdot e2t \cdot e3t} dt, \quad (1)$$

where  $dt$  is model time step (unit:  $s$ ),  $v$  is the normal to section velocity (meridional velocity in our case, unit:  $m/s$ ),  $e1v$  is the along-section grid size (at V point, unit:  $m$ ), and  $e3v$  is the cell thickness (at V point, unit:  $m$ ); similarly,  $e1t$ ,  $e2t$ , and  $e3t$  are the grid sizes but at T point. Thus,  $\Delta C$  is a unitless quantity.

In addition, only the water mass flowing into the Arctic Ocean direction is tagged. No additional criteria, for example, temperature/salinity ranges, are applied here. The return flow or eddies can lead PW to be retagged. It is ignored in this study for the simplicity of tracer design.

To better show the pathway of PW, vertical integrated tracer concentration flux vector,  $\overrightarrow{UC}_{flux}(x, y)$  from depth  $z = z_0$  to  $z = z_1$ , is defined as

$$\overrightarrow{UC}_{flux}(x, y) = \int_{z_0}^{z_1} C(x, y, z) \vec{U}(x, y, z) dz, \quad (2)$$

where  $C(x, y, z)$  is the concentration of passive tracer and  $\vec{U}(x, y, z)$  is the horizontal velocity vector. In this study,  $z_0$  is set to the depth of 200 m, and  $z_1$  is set to the surface, unless otherwise stated.

## 2.3. Oceanic Freshwater-Related Calculations

Following Aagaard and Carmack (1989) and Serreze et al. (2006), the FWC (unit:  $m$ ) is defined as

$$FWC = \int_{z_2}^0 \frac{S_{ref} - S}{S_{ref}} dz, \quad (3)$$

where  $S_{ref}$  is the reference salinity and  $S$  is the simulated 3-D salinity field.  $S_{ref}$  is set to 34.8 in this study.  $z_2$  is the lower interface of integration, and it could be a constant value (e.g., a fixed 200-m depth) or a isohaline interface (e.g., 34.8 isohaline).

If the  $FWC$  is integrated over a horizontal area ( $A$ ), it results in the volume of freshwater or freshwater storage ( $FW_{storage}$ ):

$$FW_{storage} = \iint_A FWC dA \quad (4)$$

The rate of freshwater volume, that is, freshwater flux ( $FW_{fluxsec}$ ), passing through a section is defined as

$$FW_{fluxsec} = \int_0^L \int_{z_0}^{z_1} \frac{S_{ref} - S}{S_{ref}} U_n dz dl, \quad (5)$$

where  $U_n$  is the velocity perpendicular to the section and  $L$  is the length of the section. The accumulated (integrated over time) freshwater flux, namely, freshwater transport, is to measure the change of freshwater volume caused by the lateral flow over a certain period.

The ocean surface stress, a combination of wind-ocean stress and ice-ocean stress (e.g., Yang, 2006), along a section can lead to cross-section volume flux, namely, Ekman transport ( $ET_{ekman}$ ):

$$ET_{ekman} = \int_0^L \frac{\tau_{along}}{\rho_0 f} dl, \quad (6)$$

where  $\tau_{along}$  is the along-section component of ocean surface stress,  $f$  is the Coriolis parameter, and  $\rho_0 = 1,035 \text{ kg/m}^3$  is seawater density (note that a constant value leads to only few percentages differences in the calculation compared to a temporal-variable value). A positive value means that the flow travels from left to right of the section.

Similarly, the Ekman-induced freshwater flux ( $FW_{ekman}$ ) can be calculated as follows:

$$FW_{ekman} = \int_0^L \frac{S_{ref} - S_{Ek}}{S_{ref}} \frac{\tau_{along}}{\rho_0 f} dl, \quad (7)$$

where  $S_{Ek}$  is the mean salinity within the Ekman layer. A constant Ekman depth of 20 m is assumed here as Yang (2006).

### 3. Results

#### 3.1. PW Pathways and FWC Spatial Distribution

Once PW passes the Bering Strait, it takes about 1 year to travel through the Chukchi Sea and about a total of about 7 years to flow out of the Arctic Ocean (Hu & Myers, 2013). The passive tracer in the first few years can be used to show the propagation of PW but should not be considered to show its mean circulation in the Arctic Ocean. Thus, the vertical integrated PW passive tracer concentration flux vectors (equation (2)) over 2010 to 2014 are considered here (arrows in Figure 2). The last 2 years are not considered here because the FWC seems to be in a different state from the previous 5 years (more details discussed in later sections).

It is clear that PW circulation in the Arctic Ocean is dominated by a basin-scale anticyclonic circulation (Figures 2a and 2b). This circulation pattern is bounded by the Transpolar Drift to the north, the CAA to the east, and Alaskan coast to the south, covering a much larger area than the traditional BG region. When PW travels through the Chukchi Sea, it turns right generally (1) along the Alaskan coast and (2) toward the northern/northeastern Chukchi Sea shelf. Note the majority of PW along the former route eventually enters the deep basin and turns to the left, merging into the large-scale anticyclonic circulation. High concentrations of PW can enter the deep basin via Barrow Canyon (e.g., Figures 2a–2d), which is consistent with previous observations (e.g., Itoh et al., 2013; Weingartner et al., 2017) and modeling studies (e.g., Watanabe, 2011).

Along the shallow Alaskan coast route, PW is always present, but the amount is much smaller compared to the total PW entering the Arctic Ocean. PW also joins the large-scale anticyclonic circulation after passing the northern/northeastern Chukchi Sea shelf along the second route.

The general features of PW circulation in the Arctic Ocean from the two simulations are similar (Figures 2a and 2b). PW flowing out of the Arctic Ocean, either via Fram Strait, Nares Strait, or the CAA channels, is mainly through the Transpolar Drift. It also shows that PW entering the CAA through the gates along the northern coast is mainly the return flow of the Transpolar Drift. This means that the age of PW found within the CAA will be relatively older (Hu & Myers, 2013). However, the higher-resolution simulation (ANHA12) tends to generate a stronger and tighter circulation in a more round shape within the BG. It also shows that PW can flow further westward, beyond 180° E line to the north of Chukchi Sea (Figure 2b), which is related to an expansion of the BG since 2013 (discussed in section 3.3).

Same as Hu and Myers (2013), the boundary of PW along the Transpolar Drift route matches the FWC contour (7–8 m, light blue). FWC here is defined with a reference salinity of 34.8 and integrated from the surface to the 34.8 isohaline interface. On one hand, it suggests that the spatial distribution of the freshwater in the Arctic Ocean deep basin is associated with the spreading of PW (Figures 2c and 2e; Figures 2d and 2f). On the other hand, it shows that a certain portion of PW never accumulates within the interior of the BG, implying that the changes in FWC are not directly caused by PW. Previous studies also identified other processes that can influence the BG FWC, such as atmospheric circulation or ice melting (e.g., Roy et al., 2015; Wang et al., 2018). As a result, it can affect the pathway of PW in the Arctic Ocean (Hu & Myers, 2013; Mizobata et al., 2016).

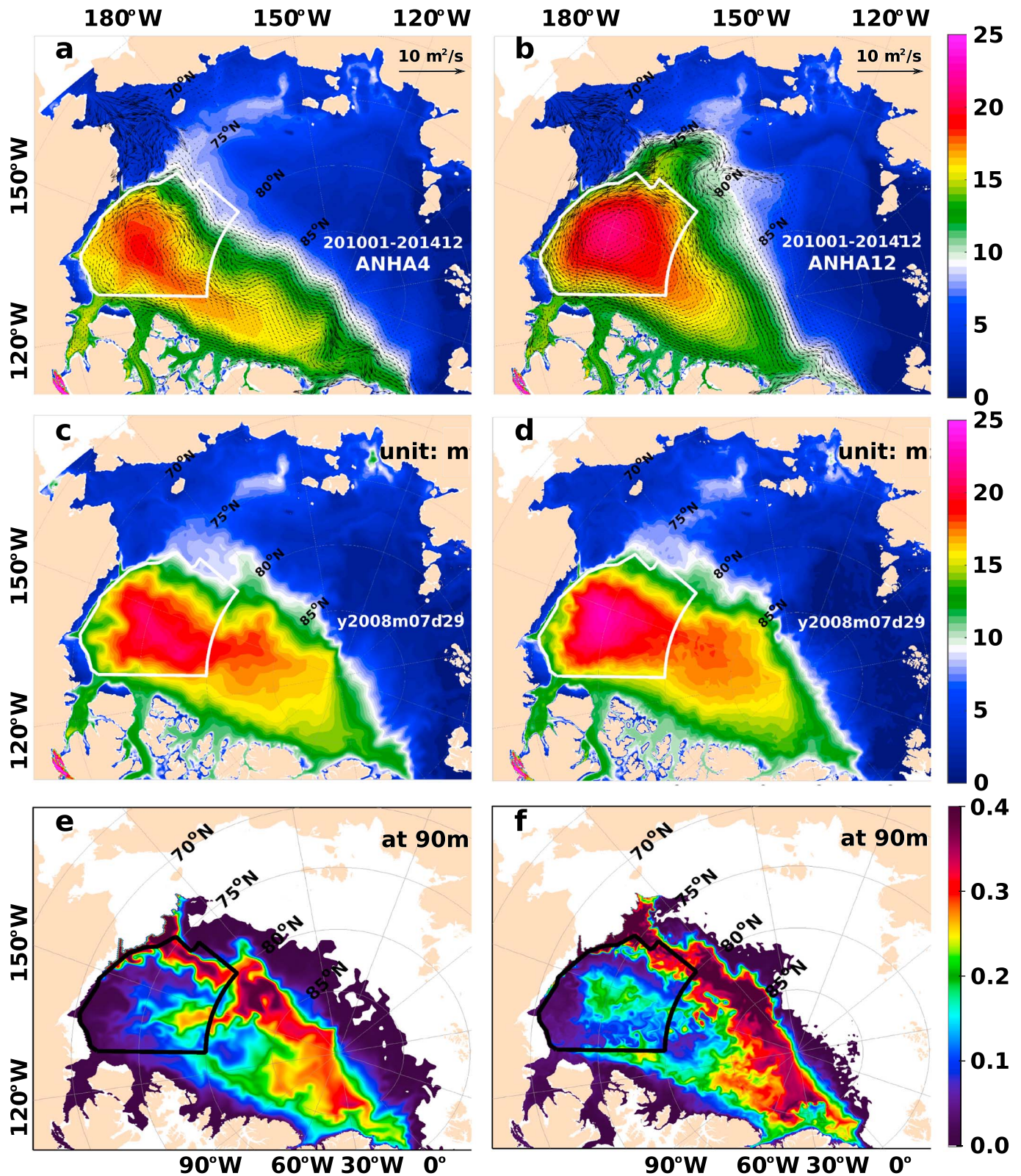


**Figure 2.** Top row: the vertical integrated Pacific Water tracer flux vectors (arrows, unit:  $\text{m}^2/\text{s}$ ) averaged over 2010–2014 in ANHA4 (a) and ANHA12 (b). Colors show the freshwater content (unit: m) integrated from surface to 34.8 isohaline surface. Middle row: “snapshot” of freshwater content computed using the model output on 29 July 2008 in ANHA4 (c) and ANHA12 (d). Bottom row: spatial distribution of Pacific Water tracer concentration at the depth of 90 m on 29 July 2008 in ANHA4 (e) and ANHA12 (d). White (black) polygon in each figure shows the location of the Beaufort Gyre region in later calculations. ANHA = Arctic Ocean and the Northern Hemisphere Atlantic.



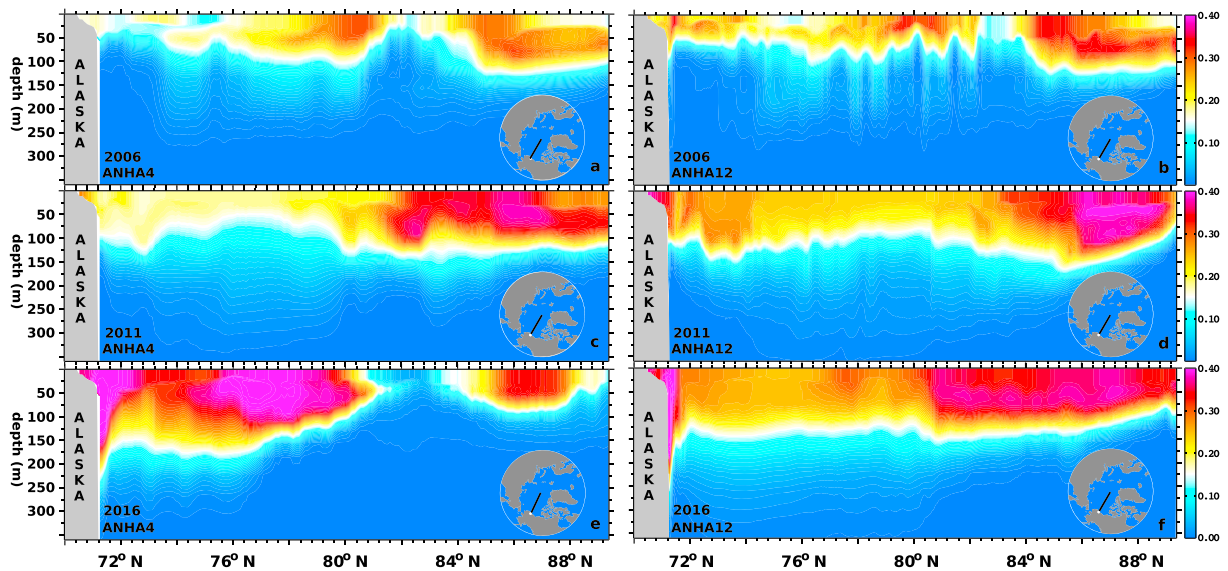


**Figure 3.** Annual mean Pacific Water tracer concentration along the 150° W section (black solid line shown in the inserted map) from ANHA4 (left column) and ANHA12 (right column) in the years of 2006 (top), 2011 (middle), and 2016 (bottom). Note that these plots are mainly used to present to what depth the Pacific Water can reach. The difference between the two simulations should be considered with caution because the horizontal shifting of the Pacific Water path can result in a large difference in tracer concentration along a single section. ANHA = Arctic Ocean and the Northern Hemisphere Atlantic.

### 3.2. PW Tracer Along 150° W Section

To show the vertical distribution of PW in the Arctic Ocean, the passive tracer concentration along the 150° W section is presented in Figure 3. The annual means of 2006, 2011, and 2016 are chosen to show the evolution of PW tracer in time. It suggests that PW passing through Bering Strait in 2002 has reached the North Pole by the end of 2006 (Figures 3a and 3b), meaning a travel time of less than 5 years. A discontinuity occurs around 80° N, related to the wavy pathway of PW (Figure 2).

In the vertical, PW mainly stays within the upper 200-m layer. The deepest penetration of PW is found along the Alaskan shelf break (Figures 3e and 3f). The core of PW along the Transpolar Drift is shallower than 100 m. A northward shoaling of PW layer is likely to be present (Figures 3e and 3f) but may have significant interannual variability.

Significantly differences in PW along this section between ANHA4 and ANHA12 are developed in later years (Figures 3c to 3f). ANHA4 obtains larger year-to-year variations (Figures 3a, 3c, and 3e), while ANHA12 obtains a relatively stable pattern with tracer gradually penetrating deeper in the BG (up to 80° N) and propagating northward (Figures 3b, 3d, and 3f), but not necessarily along the 150° W section. This is the result of a combination of differences in travel time and spatial spreading in the two simulations. The difference in spatial spreading is also evidenced in a “snapshot” of PW passive tracer distribution at 90 m on 29 July 2008 (Figures 2e and 2f).

### 3.3. FWC Variation in the Upper 200 m of the BG

As the freshwater storage within the BG plays an important role in Arctic Ocean circulation, particularly in the upper ocean, a freshwater budget within the BG is analyzed in detail here. Following Proshutinsky et al. (2009) and Krishfield et al. (2014), the BG region is defined as an area bounded by two meridians (170° W and 130° W) and two parallels (70° N and 80° N) with a water depth deeper than 300 m (Figure 4).

Figure 5 shows the spatial averaged BG FWC (integrated from surface to the 34.8 isohaline) produced by ANHA4, ANHA12, and the summertime observations obtained from the Beaufort Gyre Exploration Project website (<http://www.whoi.edu/website/beaufortgyre>). More details about the observations are described in Proshutinsky et al. (2009). The two simulations produce a similar seasonal cycle. Usually, the annual peak is in fall, that is, late October to early December; however, more recently, it occurs earlier after 2009, for example, up to the beginning of September in 2012. The annual minimum is in mid-May to early June. The interannual variation is very similar in both ANHA4 and ANHA12 until the end of 2007, and ANHA4 fails to maintain a high FWC state after that. ANHA12 reproduces a similar interannual variation as the



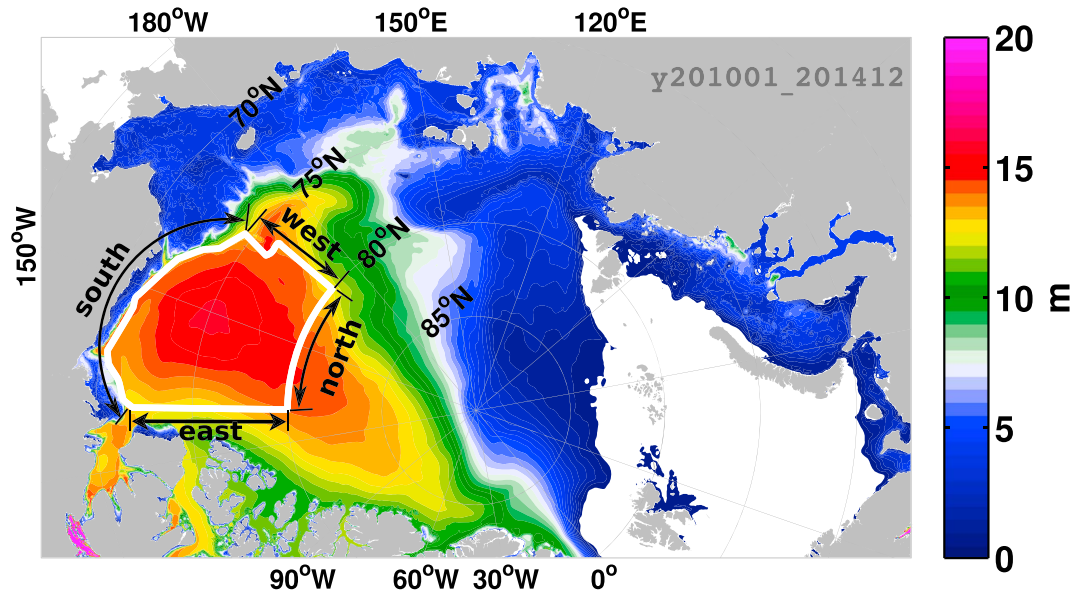


**Figure 4.** Location of the Beaufort Gyre region and sections (east, south, west, and north) defined for lateral freshwater flux calculation. Background colors show the freshwater content ANHA12 over 2010–2014 (similar to Figure 2b but integrated from surface to 200-m depth). ANHA = Arctic Ocean and the Northern Hemisphere Atlantic.

observations, with high accumulation events in 2004/2005, 2007/2008, and recent years in 2014, 2015, and 2016, and strong release events in 2012–2013. However, the simulated interannual variation is weaker than the observed, similar to another numerical study by Wang et al. (2018). It is worth noting that although ANHA4 has a lower mean BG FWC, it still obtains a similar increasing trend since 2014. This suggests that both ANHA12 and ANHA4 include common physical processes for the variations of FWC.

In both simulations, the lower BG FWC can be partly attributed to the lower freshwater state in the initial condition derived from the GLORYS2v3 product. Another possible reason is that both simulations overestimate the sea ice. Both Roy et al. (2015) and Wang et al. (2018) found that sea ice melting, locally and outside of the BG, can significantly increase the liquid freshwater accumulated in the BG. In our case, both ANHA4 and ANHA12 produce more than observed sea ice (concentration and thickness) in the BG (Figures S1–S4). While ANHA12 captures a reasonable depth of isohalines (i.e., 32.5 and 33.1) and their main interannual variations (Figures S7–S9), a positive salinity bias is found in the near surface layer at Site D (Figure S9). In addition, in our simulations, the warm temperature signal in the Atlantic Water layer is not as strong as the

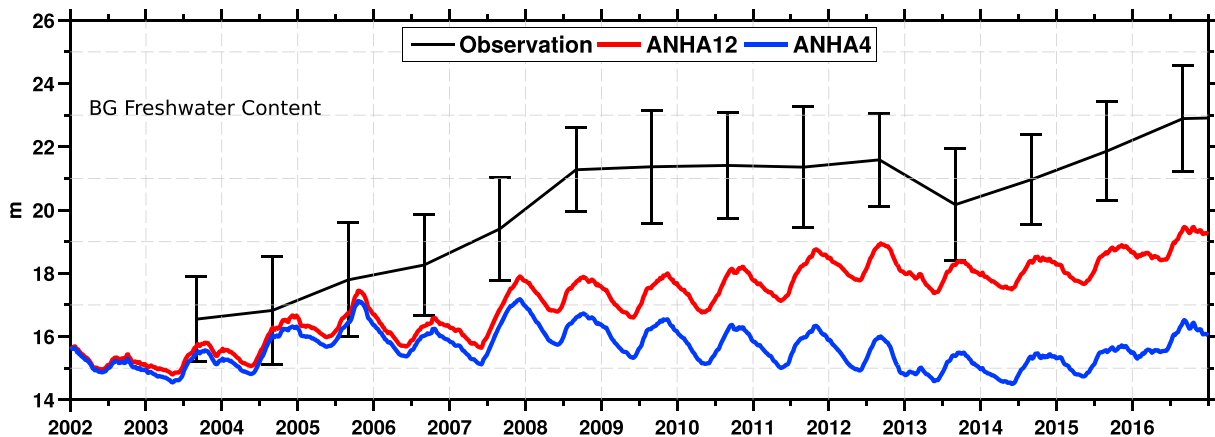


**Figure 5.** Observed (black, error bar showing the root-mean-square error) and simulated (red: ANHA12; blue: ANHA4) freshwater content (FWC; unit: m) averaged over the Beaufort Gyre (BG) region (Figure 4). The modeled FWC is 5-day averaged, while the observation is for summertime only. The FWC is calculated from integration through surface to 34.8 isohaline, relative to a reference salinity of 34.8. Details about the observation and error estimate can be found in Proshutinsky et al. (2009). ANHA = Arctic Ocean and the Northern Hemisphere Atlantic.

observed and is fading out as the integration moves forward. This is largely caused by the bias in the initial condition and the overestimation of sea ice. The coarse vertical resolution (greater than 50 m below 266 m) may also impact the simulation of the Atlantic Water layer. One other possible cause is problems in vertical mixing, both physical and numerical. Previous studies have demonstrated the impacts of vertical mixing parameterization on the BG FWC (Zhang & Steele, 2007) and the Atlantic Water layer (Golubeva & Platov, 2007). Finally, at the end of the summary section, we point out that FWC bias may also be related to model's insufficient resolution to resolve eddies.

Further model improvements are needed in the future to reduce model bias. It should be noted that ANHA12 generally captures the observed SSH patterns and interannual variation (Figures S5–S6), at least prior to 2010. In addition, ANHA4 and ANHA12 both contain bias in the initial condition and overestimate sea ice, but the focus of our analysis is on the difference between the two solutions.

### 3.4. Budget Analysis of the BG FWC

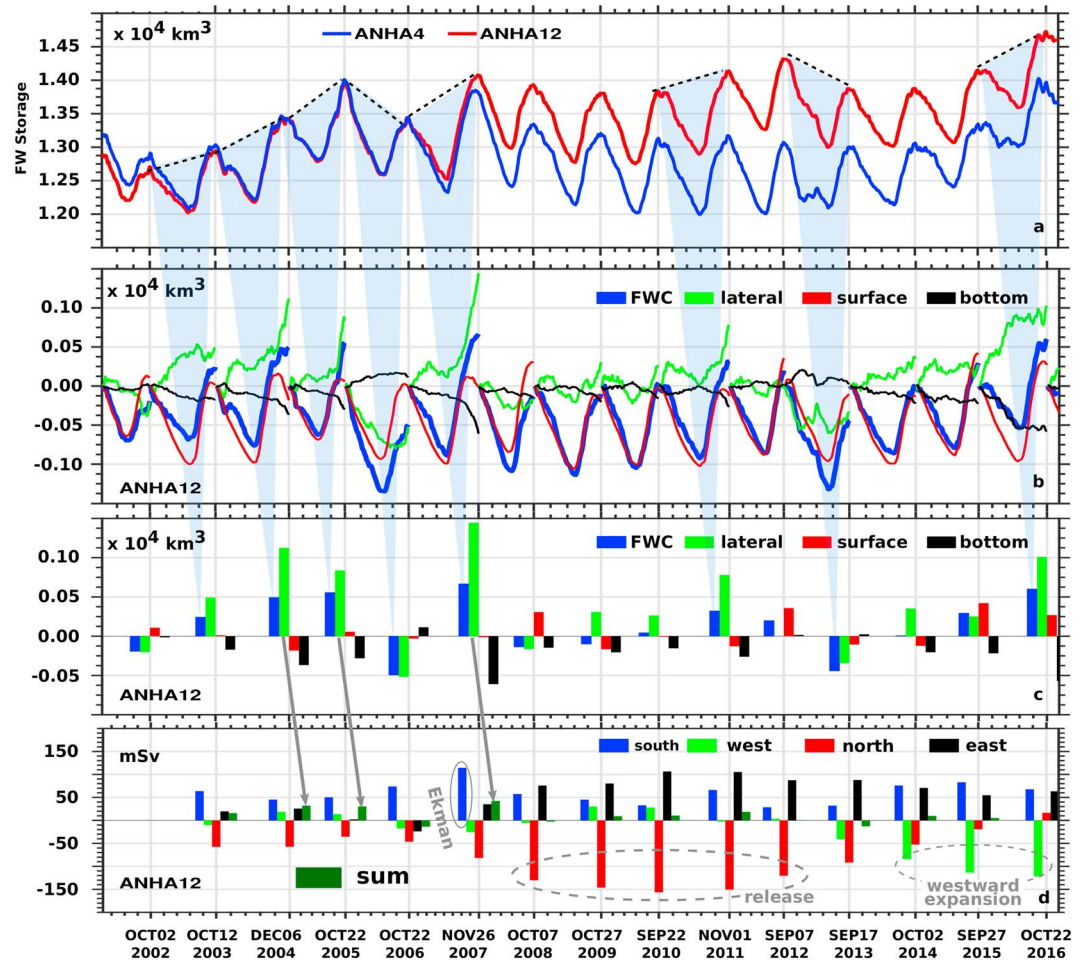
Next we analyze the budget of the BG freshwater, with the FWC calculated for the upper 200 m (Figure 6a), instead of from the surface to 34.8 isohaline (Figure 5). With this fixed control volume, the FWC variations are caused by three main components: surface freshwater processes (precipitation minus evaporation and ice melting/freezing), lateral advection, and vertical advection through the bottom interface. The contribution from lateral and vertical mixing is estimated to be small. The deepening or shoaling of the isohaline can be inferred from the third term.

Focusing on the peak-to-peak seasonal cycle in ANHA12, the seasonality of the BG FWC is dominated by the surface freshwater process (Figure 6b, red), mainly caused by ice formation and melting. The accumulated contribution of this term is usually close to zero, except in 2008, 2012, and 2015. On the interannual scale, the FWC variation is mainly due to lateral advection (Figure 6c, green bars). Freshwater accumulation events (in 2004, 2005, 2007, and 2016) are associated with a large positive lateral inflow of freshwater. Lateral advection can also function as a freshwater sink, for example, in 2006 and 2013.

In general, the lateral advection and vertical advection at the bottom interface contribute oppositely to the upper layer freshwater storage; that is, the import of freshwater due to lateral advection corresponds to downward transport through the bottom interface (e.g., in 2004, 2007, and 2016), and vice versa (e.g., in 2006). In the former case, the lateral FW input is usually larger than the release at the bottom. Thus, lateral advection not only leads to freshening in the upper layer but also provides the freshwater exported from the upper layer into the deep layer, resulting in the sublayer freshening. In the latter case, however, the upward transport of freshwater rarely happens. The event in 2008 is uncommon, as the upper layer loses freshwater through both lateral advection and saltier water imported from the sublayer.

Figure 6d shows the contribution of total lateral advection decomposed into four sections (south, west, north, and east; Figure 4). The southern section is always a freshwater source for the BG during the whole simulation period. The most pronounced event occurs in 2007 when a significant amount of freshwater is advected into the BG in fall, leading the BG freshwater storage to be in a remarkable high stage. Further analysis (Figure 7) shows that this advection event is attributed to the wind-induced Ekman transport, particularly through the southern section. Similar cases are found in 2014, 2015, and 2016 (Figures 6d and 7b). About 30–50% of the freshwater flux through the southern section can be explained by Ekman transport when strong freshwater input events happen there, for example, 58 mSv of 114 mSv in 2007, 21 mSv of 75 mSv in 2015, 26 mSv of 83 mSv in 2015, and 35 mSv of 67 mSv in 2016.

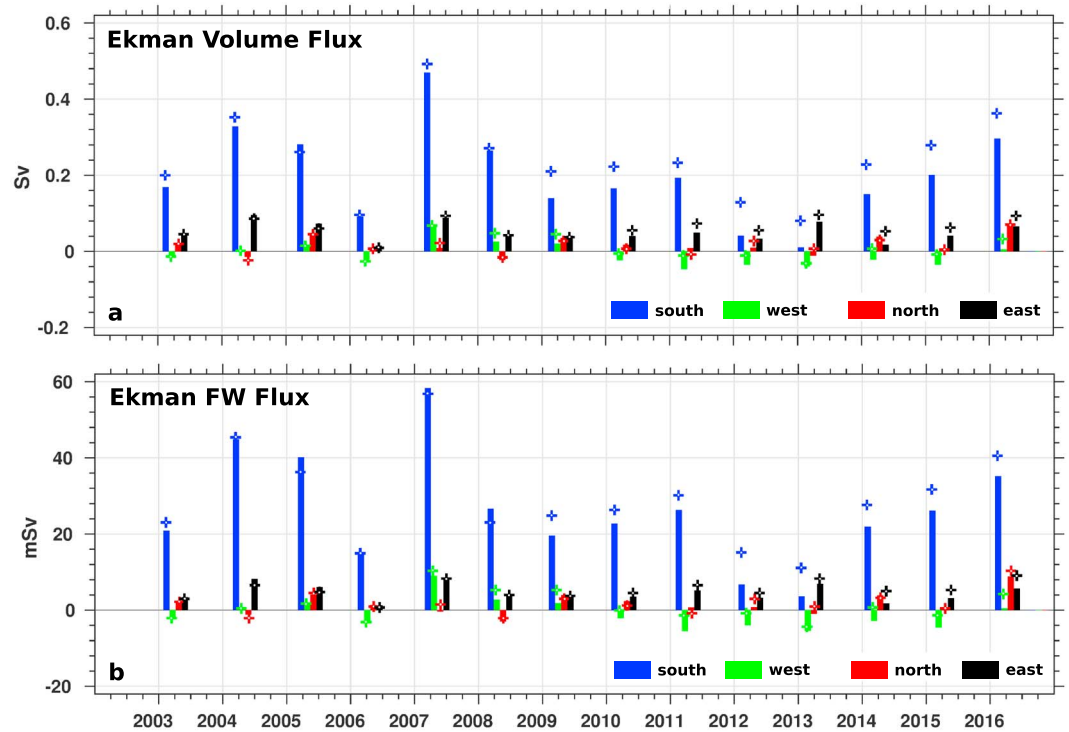
Freshwater flowing into the BG via the western section is much smaller than that via the southern section (Figure 6d). However, since 2013, a considerable amount of freshwater is exported out of the BG through the western section. Most freshwater released from the BG is through the northern section and then joins the Transpolar Drift. Interestingly, advection at the eastern section is an important source for the BG FWC, which corresponds to the return flow of the large-scale anticyclonic circulation. This component is particularly significant after 2007. As a whole, although the BG FWC is always in a high state after 2007, two freshwater release events are simulated in ANHA12: One occurs over 2008–2012 from the northern section, and the other one occurs after 2013 through the westward expansion of the BG. The westward expansion is consistent with PW pathway in Figure 2b. In a previous study, Mizobata et al. (2016) also found more Pacific-origin water transported westward during 2013/2014.



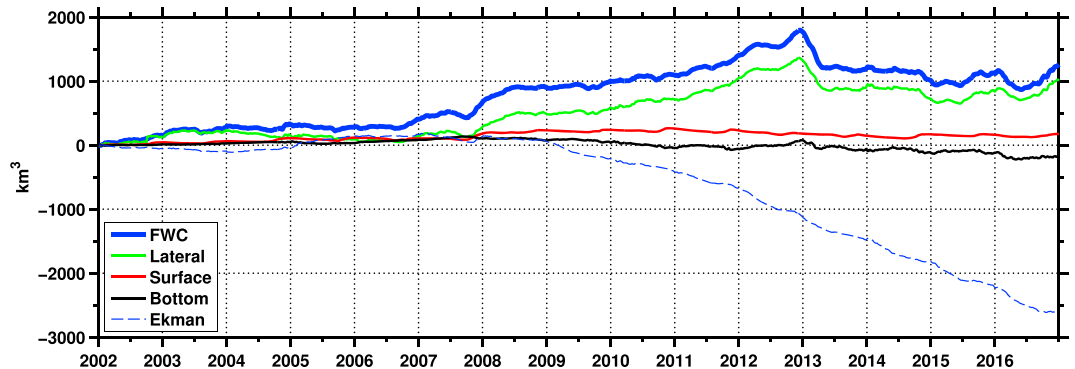
**Figure 6.** (a) Freshwater storage (unit:  $\text{km}^3$ ) of the upper 200 m within the Beaufort Gyre (BG) region (polygon defined in Figure 4) in ANHA12 (red) and ANHA4 (blue). Dashed lines and shadings highlight the seasons (from the maximum value to the maximum in the following year) with large freshwater change. (b) Seasonal changes of freshwater storage (blue, unit:  $\text{km}^3$ ) and the contributions due to lateral advection (green), surface dilution/distillation (red), and vertical advection at bottom (200 m, black) in ANHA12. Each term is the accumulated freshwater flux over the BG freshwater storage peak-to-peak period in Figure 6a. (c) Similar to (b) but on an annual basis. (d) Contribution of lateral freshwater flux (unit:  $\text{mSv}$ ,  $1 \text{ mSv} \equiv 10^3 \text{ m}^3/\text{s} \approx 31.5 \text{ km}^3/\text{year}$ ) through each BG section (defined in Figure 4). The color scheme is blue for the south, green for the west, red for the north, and black for the east. ANHA = Arctic Ocean and the Northern Hemisphere Atlantic; FWC = freshwater content.

Figure 8 shows the accumulated difference in the BG freshwater storage between ANHA12 and ANHA4. Starting from 2002, the discrepancy gradually increases to  $\sim 300 \text{ km}^3$  at the end of 2004 and maintains this level till the fall of 2006. After that, the discrepancy rapidly increase to  $\sim 670 \text{ km}^3$  at the beginning of 2008 and to  $\sim 1,800 \text{ km}^3$  by the end of 2012 and falls back to  $\sim 1,260 \text{ km}^3$  at the end of 2016 (Figures 6a and 8). The discrepancy can be mainly attributed to the differences in lateral advection (Figure 8). Differences in the accumulated surface fluxes and vertical advection through the bottom interface are much smaller. The small difference in the surface freshwater input is due to the similar ice formation/melting in the two simulations. Hu et al. (2018) previously found that model horizontal resolution at such scales only plays a small role in sea ice simulation.

The lateral freshwater input due to Ekman transport between the two simulations shows small difference prior to 2009 (Figure 8), hence is not the cause of the BG FWC discrepancy during this period. Since 2009, ANHA4 obtains significantly more freshwater into the BG due to the Ekman component, mainly through the souther section (Figures 7 and 8). This is opposite to the trend of more freshwater accumulation in ANHA12 than in ANHA4. Hence, the discrepancy in the Ekman component is the consequence, rather than the



**Figure 7.** Ekman-induced volume flux (a, unit: Sv,  $1 \text{ Sv} \equiv 10^6 \text{ m}^3/\text{s}$ ) and freshwater flux (b, unit: mSv,  $1 \text{ mSv} \equiv 10^3 \text{ m}^3/\text{s} \approx 31.5 \text{ km}^3/\text{year}$ ) crossing four lateral sections of the Beaufort Gyre region (defined in Figure 4) in ANHA12 (bars) and ANHA4 (plus-sign markers). The color scheme is blue for the south, green for the west, red for the north, and black for the east. The fluxes are averaged over each Beaufort Gyre freshwater storage peak-to-peak period each year (shown in Figure 6a). ANHA = Arctic Ocean and the Northern Hemisphere Atlantic; FW = freshwater.



**Figure 8.** Accumulated differences (ANHA12 minus ANHA4) in the Beaufort Gyre FWC (blue) due to lateral freshwater flux (green), surface dilution/distillation (red), and vertical advection at bottom (200 m, black) from 1 January 2002. The dashed blue line represents the accumulated freshwater difference induced by the Ekman transport. It is included for comparison but not a part of the freshwater budget analysis. ANHA = Arctic Ocean and the Northern Hemisphere Atlantic; FWC = freshwater content.

cause of the BG FWC discrepancy between the two simulations. The non-Ekman component of the lateral freshwater transport is the primary reason of more freshwater accumulated within the BG in ANHA12.

Difference in horizontal freshwater advection through each section of the BG is also analyzed (figures not shown). Basically, it is found that the larger lateral freshwater advection in ANHA12 is related to the tighter and stronger BG, which leads to less freshwater exported via the northern section and more freshwater imported through the eastern section. Lateral advection through the southern section actually plays an opposite role, that is, less freshwater into the interior from this section in ANHA12 compared to ANHA4. This



is consistent with the Ekman transport analysis (Figure 7). ANHA12 obtains a rapid increase of freshwater release from the western section after 2012, associated with the westward extension of the BG (Figure 6d).

### 3.5. Difference in the Lateral Freshwater Flux Due to Slow-Varying Circulation and Eddies

Consistent with the analysis of lateral freshwater flux, PW tracer flux vectors (Figures 2a and 2b) also show a tighter and stronger BG in ANHA12. This raises the question to answer: Why can ANHA12 produce an intensified anticyclonic circulation that leads to less export of freshwater through the northern section and more import through the eastern section of the BG? To answer this question, we need to differentiate roles played by mean circulation and eddies.

The total lateral freshwater flux is decomposed into the slow-varying and fast-varying (eddy) components. The two components are computed according to equation (5) but using  $\bar{S}$ ,  $\bar{U}_n$ , and  $S'$ ,  $U'_n$ . Here  $S$  and  $U_n$  are decomposed into  $S = \bar{S} + S'$ ,  $U_n = \bar{U}_n + U'_n$ , where  $\bar{S}$  and  $\bar{U}_n$  denote the 3-month running mean and  $S'$  and  $U'_n$  represent the residual.

Prior to 2005, the two simulations show small differences in the slow-varying and eddy components of the lateral freshwater flux (Figure 9). Overall, the eddy component in ANHA12 contributes more to the BG freshwater accumulation than in ANHA4. This can be attributed to stronger eddy activities resolved by ANHA12. Figure 10 shows the upper 200-m layer eddy kinetic energy (EKE) during June 2004 to December 2004 for the two simulations. EKE here is also calculated using velocity fluctuations obtained with a 3-month running mean. ANHA12 obtains higher EKE band around the boundary of BG and also in the interior.

Starting from 2005, ANHA12 obtains more input of the BG freshwater due to the slow-varying component, and more lateral release of freshwater due to eddies. During this period, EKE around the boundary of the BG is still larger in ANHA12 than in ANHA4 (figure not shown). It is very interesting to note that the significantly more freshwater accumulated in the BG in ANHA12 is due to the difference in lateral input by slow-varying motion, instead of due to the difference in the eddy component prior to 2005. This time evolution of eddy effects may suggest that the model is undergoing spin-up from the initial state. On the other hand, it also suggests the importance to resolve eddies in modeling the BG FWC variability.

The ability of large-scale ocean numerical models to resolve eddies can be estimated by comparing model horizontal resolution with the first baroclinic Rossby deformation radius ( $R_0$ ; Chelton et al., 1998; Nurser & Bacon, 2014).  $R_0$  is defined as the vertical integral of buoyancy frequency ( $N$ ) scaled by  $|f| * \pi$  (equations 4 and 5 in Nurser & Bacon, 2014). The software package of CDFTOOLS (<https://github.com/meom-group/CDFTOOLS>) is used to perform the calculation.

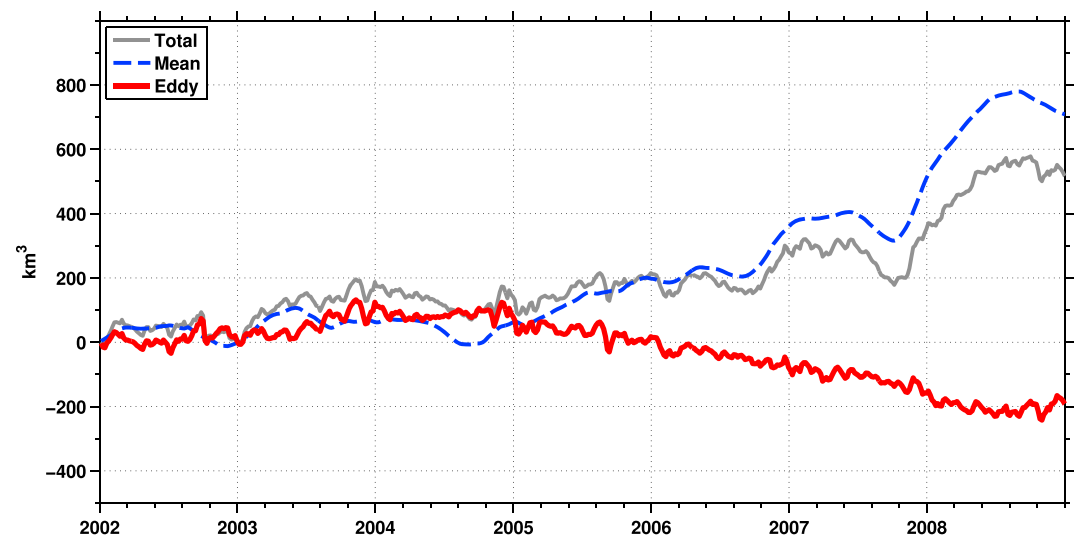


**Figure 9.** Difference (ANHA12 minus ANHA4) in the accumulated total (gray), slow-varying (dashed blue), and eddy (red) components of lateral freshwater flux (unit:  $\text{km}^3$ ) along the boundary of the Beaufort Gyre region (defined in Figure 4) over the top 200-m layer. ANHA = Arctic Ocean and the Northern Hemisphere Atlantic.

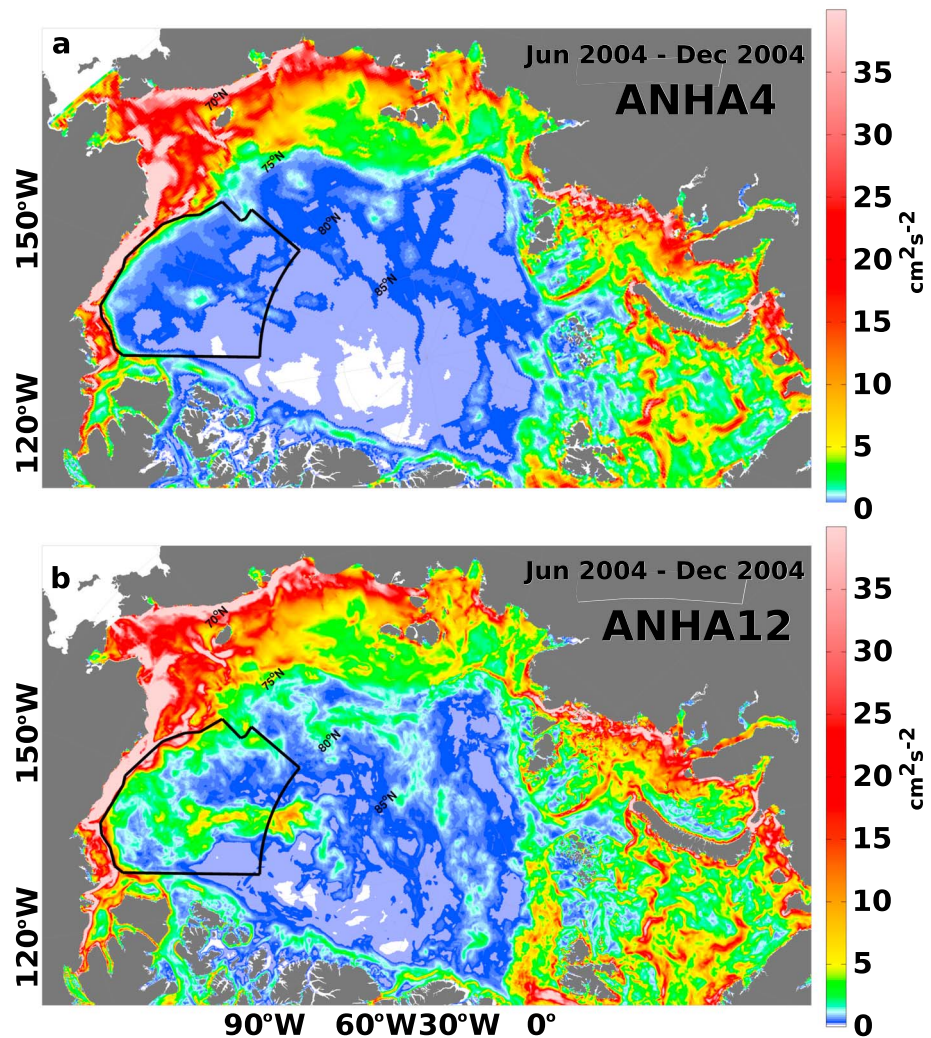


**Figure 10.** Upper 200-m eddy kinetic energy (unit:  $\text{cm}^2/\text{s}^2$ ) averaged over June to December in 2004 for ANHA4 (a) and ANHA12 (b). ANHA = Arctic Ocean and the Northern Hemisphere Atlantic.

To resolve an eddy, at least two grid points per eddy radius are required. Here the “effective grid spacing” is defined as the grid-diagonal distance following Hallberg (2013):

$$l = \sqrt{e1t^2 + e2t^2}, \quad (8)$$

where  $e1t$  and  $e2t$  are model grid size in zonal and meridional direction, respectively. The ratio of  $R_0$  to  $l$  is presented in Figure 11 (a for ANHA4 and b for ANHA12) over the same period as the EKE analysis. In this study, eddy resolving is defined as  $R_0/l \geq 2$ , and eddy permitting as  $R_0/l \approx 1$ . It is clearly evidenced that ANHA12 is roughly eddy resolving within the BG (Figure 11b). These eddies are well illustrated by PW tracer in Figures 2e and 2f. In comparison, ANHA4 is barely eddy permitting (Figure 11a) based on this criterion. In order to exclude the impact of  $R_0$  difference between ANHA4 and ANHA12, the time series of  $R_0$  is also calculated (Figure 11c). Both ANHA4 and ANHA12 show  $R_0$  has a clear seasonal cycle with an amplitude  $\sim 0.7$  km around the mean ( $\sim 10.5$  km). The interannual variation exists, for example, an increase of  $\sim 0.5$  km in 2015 and 2016, but these variations are not significant compared to the mean value. The difference in  $R_0$  between the two simulations is also negligible, resulting in this ratio being controlled by the model effective grid spacing.

In previous studies, the stability of the BG has also been linked to the mesoscale eddy activity (e.g., Doddridge et al., 2019; Manucharyan & Spall, 2016; Manucharyan et al., 2016). Therefore, we propose that model

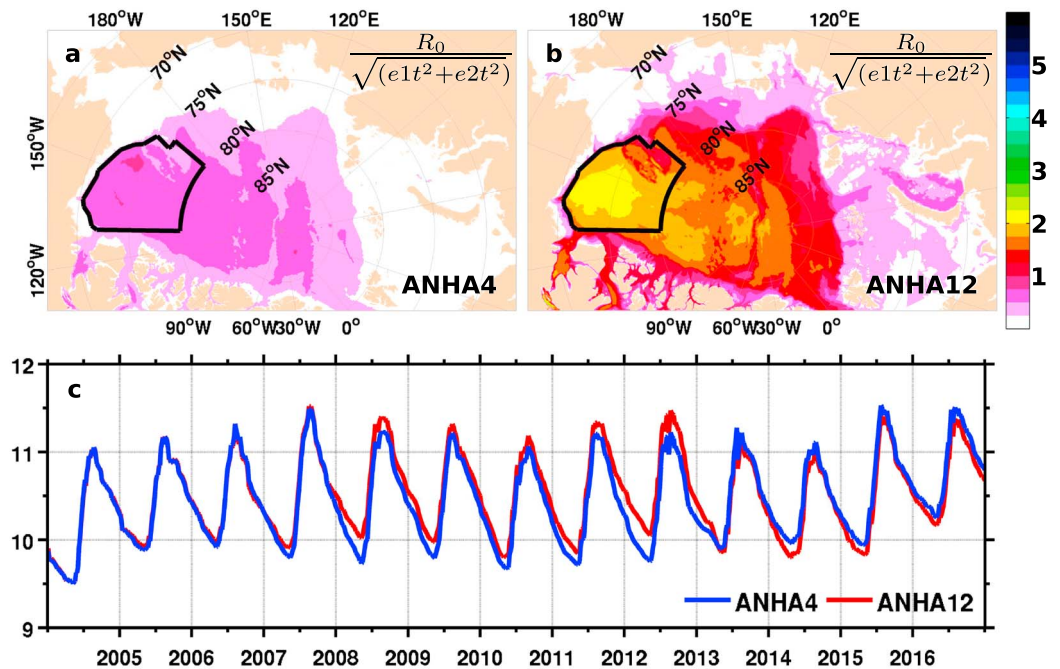


**Figure 11.** Ratio of the first baroclinic Rossby radius ( $R_0$ ) to model cell diagonal length ( $l = \sqrt{e1t^2 + e2t^2}$ ,  $e1t$ , and  $e2t$  are zonal and meridional grid size, respectively) in ANHA4 (a) and ANHA12 (b).  $R_0$  is averaged over June 2004 to December 2004, the same as the eddy kinetic energy calculation period in Figure 10. (c) Time series of  $R_0$  (unit: km) in Beaufort Gyre region (defined in Figure 4) over January 2004 to December 2016. ANHA = Arctic Ocean and the Northern Hemisphere Atlantic.

horizontal resolution does play an important role in simulation of the BG freshwater system. In return, the horizontal distribution of the BG FWC can affect the anticyclonic circulation, and thus the spreading of PW.

#### 4. Summary and Discussion

This work is a follow-on to Hu and Myers (2013). As discussed in section 1, that work (Hu & Myers, 2013) showed that the spatial distribution of the freshwater within the Canada Basin sets the pathways for PW. Based on that, they argued that the coastal Alaskan route for PW is only present during periods of a weak BG, while the Transpolar Drift route is dominating when the BG is strong and deep. Here we carry out a more realistic study than Hu and Myers (2013) with the model being able to simulate a high FWC situation and interannual variability.

The simulated PW circulation in the Arctic Ocean is dominated by a basin-scale anticyclonic circulation. This circulation covers a much larger area than the traditional BG, being bounded by the Transpolar Drift to the north, the CAA to the east, and the Alaskan coast to the south. Consistent with previous observational (e.g., Itoh et al., 2013; Weingartner et al., 2017) and modeling studies (e.g., Watanabe, 2011), high concentrations of PW can enter the deep basin via Barrow Canyon (e.g., Figures 2a–2d). PW also joins the large-scale anticyclonic circulation after passing the northern/northeastern Chukchi Sea shelf. Along the shallow Alaskan coast route, PW is always present, but the amount is much smaller compared to the total PW entering the Arctic Ocean. The general features of PW circulation in the Arctic Ocean are not affected by the model's horizontal resolution. After crossing the Arctic Ocean via the Transpolar Drift, PW leaves the basin via either Fram Strait, Nares Strait or the CAA channels. PW using the CAA route generally enters from the north, as part of the return flow of the Transpolar Drift.

As in Hu and Myers (2013), the boundary of PW along the Transpolar Drift route matches the FWC contour (7–8 m, light blue contours in Figures 2a and 2b). This suggests that the spatial distribution of the freshwater in the Arctic deep basin is associated with the spreading of PW (Figures 2c and 2e; Figures 2d and 2f). A certain portion of PW never accumulates in the BG, implying that the changes in FWC are not directly caused by PW rather than linked to the variations of atmospheric circulation and sea ice melting.



The seasonal cycle of FWC is similar for the two simulations with different resolutions, ANHA4 and ANHA12. The interannual variations are also similar between the two runs, but only up to the end of 2007. After 2007, ANHA4 is unable to maintain the observed high freshwater state, leading to a significant difference with ANHA12. Meanwhile, ANHA12 obtains similar interannual variations of the BG freshwater storage as observations (Figure 5), although with a smaller magnitude (Figure 5). Included in this is ANHA12 being able to represent the high accumulation events in 2004/2005, 2007/2008, and recent years (2014–2016), while also having strong release events in 2012/2013.

Focusing on the peak-to-peak seasonal cycle of the BG FWC in ANHA12, its seasonality is dominated by the surface freshwater process, due to ice formation and melting (Figure 6b) On the interannual scale, the variability is mainly attributed to the lateral advection (Figure 6c). Strong FWC accumulation events, such as in 2004, 2005, 2007, and 2016, are associated with large positive lateral inflows of freshwater. Lateral advection can also function as a freshwater sink, such as in 2006 and 2013. In general, lateral advection and vertical advection at the bottom interface contribute oppositely to the upper layer FWC. That is, inward lateral advection corresponds to downward freshwater transport through the bottom (200 m).

Differences in lateral freshwater advection is the main cause of the difference in interannual variations of the BG FWC between the two simulations (Figure 8). Difference in the Ekman component of freshwater transport is small prior to 2009 and becomes significant after 2009. As ANHA4 has more lateral freshwater input due to Ekman transport than ANHA12 (Figures 7 and 8), differences in Ekman transport are the consequence, rather than the cause of the BG FWC discrepancy between ANHA4 and ANHA12. The cause of the FWC discrepancy is the non-Ekman component related to the tighter and stronger BG in ANHA12.

Difference in lateral freshwater flux between the two simulations is decomposed into the components due to slow-varying circulation and eddies through applying a 3-month running mean to the velocity and salinity variables. The resulting time series (Figure 9) show that prior to 2005 the eddy component contributes more to the accumulation of the BG freshwater (though by a relatively small amount) in ANHA12. Starting from 2005, the significantly more freshwater accumulation in ANHA12 is due to the slow-varying component. The time evolution of both components suggests that the model is undergoing spin-up from the initial condition.

The rapid increases in difference in the BG FWC and the lateral freshwater input due to the slow-varying component are related to each other, but the causes of their increases are not obvious. The relationship of their increases with the time evolution of the eddy component is not clear. Because ANHA12 obtains the BG FWC in better agreement with observations, and it resolves stronger eddy variations than ANHA4 (Figure 10), the results of this study suggest the importance to resolve eddies in modeling the BG FWC. Lastly, as the horizontal grid spacing of ANHA12 is only about half of the first baroclinic Rossby deformation radius (Figure 11), it remains to be seen whether further increase model resolution can bring the modeled BG FWC closer to the observed magnitude. This should be explored in future studies.

## References

- Aagaard, K., & Carmack, E. C. (1989). The role of sea ice and other fresh water in the Arctic circulation. *Journal of Geophysical Research*, *94*(C10), 14,485–14,498.
- Aagaard, K., Weingartner, T. J., Danielson, S. L., Woodgate, R. A., Johnson, G. C., & Whitley, T. E. (2006). Some controls on flow and salinity in Bering Strait. *Geophysical Research Letters*, *33*, L19602. <https://doi.org/10.1029/2006GL026612>
- Aksenov, Y., Karcher, M., Proshutinsky, A., Gerdes, R., De Cuevas, B., Golubeva, E., et al. (2016). Arctic pathways of Pacific Water: Arctic Ocean model intercomparison experiments. *Journal of Geophysical Research: Oceans*, *121*, 27–59. <https://doi.org/10.1002/2015JC011299>
- Alkire, M. B., Falkner, K. K., Morison, J., Collier, R. W., Guay, C. K., Desiderio, R. A., et al. (2010). Sensor-based profiles of the NO parameter in the central Arctic and southern Canada Basin: New insights regarding the cold halocline. *Deep Sea Research Part I: Oceanographic Research Papers*, *57*(11), 1432–1443. <https://doi.org/10.1016/j.dsr.2010.07.011>
- Alkire, M. B., Falkner, K. K., Rigor, I., Steele, M., & Morison, J. (2007). The return of Pacific waters to the upper layers of the central Arctic Ocean. *Deep Sea Research Part I: Oceanographic Research Papers*, *54*(9), 1509–1529. <https://doi.org/10.1016/j.dsr.2007.06.004>
- Alkire, M. B., Morison, J., Schweiger, A., Zhang, J., Steele, M., Peralta-Ferriz, C., & Dickinson, S. (2017). A meteoric water budget for the Arctic Ocean. *Journal of Geophysical Research: Oceans*, *122*, 10,020–10,041. <https://doi.org/10.1002/2017JC012807>
- Armitage, T. W., Bacon, S., Ridout, A. L., Petty, A. A., Wolbach, S., & Tsamados, M. (2017). Arctic Ocean surface geostrophic circulation 2003–2014. *The Cryosphere*, *11*(4), 1767–1780. <https://doi.org/10.5194/tc-11-1767-2017>
- Armitage, T. W., Bacon, S., Ridout, A. L., Thomas, S. F., Aksenov, Y., & Wingham, D. J. (2016). Arctic sea surface height variability and change from satellite radar altimetry and GRACE, 2003–2014. *Journal of Geophysical Research: Oceans*, *121*, 4303–4322. <https://doi.org/10.1002/2015JC011579>
- Aumont, O., Éthé, C., Tagliabue, A., Bopp, L., & Gehlen, M. (2015). PISCES-v2: an ocean biogeochemical model for carbon and ecosystem studies. *Geoscientific Model Development Discussions*, *8*(2), 1375–1509.

## Acknowledgments

We are grateful to the comments from the two anonymous reviewers and the associate editor that helped greatly to improve the quality of this paper. We gratefully acknowledge the financial and logistic support of grants from the Natural Sciences and Engineering Research Council (NSERC) of Canada. These include a Discovery Grant (rgpin 227438-09) awarded to P. G. M., Climate Change and Atmospheric Research Grants (VITALS - RGPCC 433898 and the Canadian Arctic Geotraces program - RGPCC 433848), and Polar Knowledge (432295). We are grateful to the NEMO development team and the Drakkar project for providing the model and continuous guidance, and to Westgrid and Compute Canada for computational resources, where all model experiments were performed and are archived (<http://www.compute.ca>). We thank G. Smith for providing the CGRF forcing fields from Environment and Climate Change Canada. The Greenland freshwater flux data analyzed are that presented in Bamber et al. (2012) and are available on request as a gridded product. We acknowledge NCAR/UCAR for making the Dai and Trenberth Global River Flow and Continental Discharge Dataset available. We also thank Mercator Ocean for providing the GLORYS model output for initial and open boundary conditions. The GLORYS reanalysis project is carried out in the framework of the European Copernicus Marine Environment Monitoring Service (CMEMS). We thank the CDFTOOL project (<https://github.com/meom-group/CDFTOOLS>) for making the package available. Arctic dynamic topography data (Armitage et al., 2016) were provided by the Centre for Polar Observation and Modelling, University College London ([www.cpom.ucl.ac.uk/dynamic\\_topography](http://www.cpom.ucl.ac.uk/dynamic_topography)). The observed BG freshwater content, ice draft, temperature, and salinity profiles were collected and made available by the Beaufort Gyre Exploration Program based at the Woods Hole Oceanographic Institution (<https://www.whoi.edu/beaufortgyre>) in collaboration with researchers from Fisheries and Oceans Canada at the Institute of Ocean Sciences.



- Babb, D. G., Galley, R. J., Asplin, M. G., Lukovich, J. V., & Barber, D. G. (2013). Multiyear sea ice export through the Bering Strait during winter 2011–2012. *Journal of Geophysical Research: Oceans*, *118*, 5489–5503. <https://doi.org/10.1002/jgrc.20383>
- Bamber, J. L., Tedstone, A. J., King, M. D., Howat, I. M., Enderlin, E. M., van den Broeke, M. R., & Noel, B. (2018). Land ice freshwater budget of the Arctic and North Atlantic Oceans: 1. Data, methods, and results. *Journal of Geophysical Research: Oceans*, *123*, 1827–1837. <https://doi.org/10.1002/2017JC013605>
- Bamber, J., van den Broeke, M., Ettema, J., Lenaerts, J., & Rignot, E. (2012). Recent large increases in freshwater fluxes from Greenland into the North Atlantic. *Geophysical Research Letters*, *39*, L19501. <https://doi.org/10.1029/2012GL052552>
- Barnier, B., Madec, G., Penduff, T., Molines, J. M., Treguier, A. M., Le Sommer, J., et al. (2006). Impact of partial steps and momentum advection schemes in a global ocean circulation model at eddy-permitting resolution. *Ocean Dynamics*, *56*(5), 543–567.
- Bauch, D., Schlosser, P., & Fairbanks, R. G. (1995). Freshwater balance and the sources of deep and bottom waters in the Arctic Ocean inferred from the distribution of H<sub>2</sub>18O. *Progress in Oceanography*, *35*(1), 53–80.
- Bouillon, S., Morales Maqueda, M., Legat, V., & Fichefet, T. (2009). An elastic-viscous-plastic sea ice model formulated on Arakawa B and C grids. *Ocean Modelling*, *27*(3), 174–184.
- Broecker, W. S., Peacock, S. L., Walker, S., Weiss, R., Fahrback, E., Schröder, M., et al. (1998). How much deep water is formed in the Southern Ocean? *Journal of Geophysical Research*, *103*, 15,833–15,843. <https://doi.org/10.1029/98JC00248>
- Brugler, E. T., Pickart, R. S., Moore, G. W. K., Roberts, S., Weingartner, T. J., & Statscewich, H. (2014). Seasonal to interannual variability of the Pacific water boundary current in the Beaufort Sea. *Progress in Oceanography*, *127*, 1–20. <https://doi.org/10.1016/j.pocean.2014.05.002>
- Carmack, E. C., McLaughlin, F. A., Yamamoto-Kawai, M., Itoh, M., Shimada, K., Krishfield, R., & Proshutinsky, A. Y. (2008). Freshwater storage in the Northern Ocean and the special role of the Beaufort Gyre. *Arctic-Subarctic Ocean Fluxes: Defining the Role of the Northern Seas in Climate* pp. 145–169. Dordrecht: Springer.
- Carmack, E. C., Yamamoto-Kawai, M., Haine, T. W. N., Bacon, S., Bluhm, B. A., Lique, C., et al. (2016). Freshwater and its role in the Arctic Marine System: Sources, disposition, storage, export, and physical and biogeochemical consequences in the Arctic and global oceans. *Journal of Geophysical Research: Biogeosciences*, *121*, 675–717. <https://doi.org/10.1002/2015JG003140>
- Chelton, D. B., DeSzoeke, R. A., Schlax, M. G., El Naggar, K., & Siwertz, N. (1998). Geographical variability of the first baroclinic Rossby radius of deformation. *Journal of Physical Oceanography*, *28*(3), 433–460. [https://doi.org/10.1175/1520-0485\(1998\)028<0433:GVOTFB>2.0.CO;2](https://doi.org/10.1175/1520-0485(1998)028<0433:GVOTFB>2.0.CO;2)
- Coachman, L. K., & Aagaard, K. (1966). On the water exchange through Bering Strait. *Limnology and Oceanography*, *11*(1), 44–59.
- Coachman, L. K., Aagaard, K., & Tripp, R. B. (1975). *Bering Strait: The regional physical oceanography*, pp. 172. Seattle, WA: University of Washington Press.
- Cross, J. N., Mathis, J. T., Pickart, R. S., & Bates, N. R. (2018). Formation and transport of corrosive water in the Pacific Arctic region. *Deep Sea Research Part II: Topical Studies in Oceanography*, *152*, 67–81. <https://doi.org/10.1016/j.dsr2.2018.05.020>
- Dai, A., Qian, T., Trenberth, K. E., & Milliman, J. D. (2009). Changes in continental freshwater discharge from 1948 to 2004. *Journal of Climate*, *22*(10), 2773–2792.
- Dodd, P. A., Heywood, K. J., Meredith, M. P., Naveira-Garabato, A. C., Marca, A. D., & Falkner, K. K. (2009). Sources and fate of freshwater exported in the East Greenland Current. *Geophysical Research Letters*, *36*, L19608. <https://doi.org/10.1029/2009GL039663>
- Dodd, P. A., Rabe, B., Hansen, E., Falck, E., Mackensen, A., Rohling, E., et al. (2012). The freshwater composition of the Fram Strait outflow derived from a decade of tracer measurements. *Journal of Geophysical Research*, *117*, C11005. <https://doi.org/10.1029/2012JC008011>
- Doddridge, E. W., Meneghello, G., Marshall, J., Scott, J., & Lique, C. (2019). A three-way balance in the Beaufort Gyre: The ice-ocean governor, wind stress, and eddy diffusivity. *Journal of Geophysical Research: Oceans*, *124*, 1–18. <https://doi.org/10.1029/2018JC014897>
- Drakkar Group (2007). Eddy-permitting ocean circulation hindcasts of past decades. *CLIVAR Exchanges No 42*, *12*(3), 8–10.
- Fichefet, T., & Maqueda, M. A. M. (1997). Sensitivity of a global sea ice model to the treatment of ice thermodynamics and dynamics. *Journal of Geophysical Research*, *102*(C6), 12,609–12,646.
- Gent, P. R., & McWilliams, J. C. (1990). Isopycnal mixing in ocean circulation models. *Journal of Physical Oceanography*, *20*(1), 150–155. [https://doi.org/10.1175/1520-0485\(1990\)020<0150:IMIOCM>2.0.CO;2](https://doi.org/10.1175/1520-0485(1990)020<0150:IMIOCM>2.0.CO;2)
- Golubeva, E. N., & Platov, G. A. (2007). On improving the simulation of Atlantic Water circulation in the Arctic Ocean. *Journal of Geophysical Research*, *112*, C04S05. <https://doi.org/10.1029/2006JC003734>
- Gong, D., & Pickart, R. S. (2015). Summertime circulation in the eastern Chukchi Sea. *Deep Sea Research Part II: Topical Studies in Oceanography*, *118*, 18–31. <https://doi.org/10.1016/j.dsr2.2015.02.006>
- Grebmeier, J. M., Cooper, L. W., Feder, H. M., & Sirenko, B. I. (2006). Ecosystem dynamics of the Pacific-influenced northern Bering and Chukchi seas in the Amerasian Arctic. *Progress in Oceanography*, *71*(2-4), 331–361.
- Hallberg, R. (2013). Using a resolution function to regulate parameterizations of oceanic mesoscale eddy effects. *Ocean Modelling*, *72*, 92–103. <https://doi.org/10.1016/j.ocemod.2013.08.007>
- Hu, X., & Myers, P. G. (2013). A Lagrangian view of Pacific water inflow pathways in the Arctic Ocean during model spin-up. *Ocean Modelling*, *71*, 66–80. <https://doi.org/10.1016/j.ocemod.2013.06.007>
- Hu, X., Sun, J., Chan, T. O., & Myers, P. G. (2018). Thermodynamic and dynamic ice thickness contributions in the Canadian Arctic Archipelago in NEMO-LIM2 numerical simulations. *The Cryosphere*, *12*(4), 1233–1247. <https://doi.org/10.5194/tc-12-1233-2018>
- Hunke, E. C., & Dukowicz, J. K. (1997). An elastic-viscous-plastic model for sea ice dynamics. *Journal of Physical Oceanography*, *27*(9), 1849–1867.
- Itoh, M., Nishino, S., Kawaguchi, Y., & Kikuchi, T. (2013). Barrow Canyon volume, heat, and freshwater fluxes revealed by long-term mooring observations between 2000 and 2008. *Journal of Geophysical Research: Oceans*, *118*, 4363–4379. <https://doi.org/10.1002/jgrc.20290>
- Itoh, M., Shimada, K., Kamoshida, T., McLaughlin, F., Carmack, E., & Nishino, S. (2012). Interannual variability of Pacific Winter Water inflow through Barrow Canyon from 2000 to 2006. *Journal of oceanography*, *68*(4), 575–592.
- Jones, E. P., & Anderson, L. G. (1986). On the origin of the chemical properties of the Arctic Ocean halocline. *Journal of Geophysical Research*, *91*(C9), 10,759–10,767.
- Jones, E. P., Anderson, L. G., Jutterström, S., Mintrop, L., & Swift, J. H. (2008). Pacific freshwater, river water and sea ice meltwater across Arctic Ocean basins: Results from the 2005 Beringia Expedition. *Journal of Geophysical Research*, *113*, C08012. <https://doi.org/10.1029/2007JC004124>
- Jones, E. P., Anderson, L. G., & Swift, J. H. (1998). Distribution of Atlantic and Pacific waters in the upper Arctic Ocean: Implications for circulation. *Geophysical Research Letters*, *25*(6), 765–768.

- Krishfield, R. A., Proshutinsky, A., Tateyama, K., Williams, W. J., Carmack, E. C., McLaughlin, F. A., & Timmermans, M.-L. (2014). Deterioration of perennial sea ice in the Beaufort Gyre from 2003 to 2012 and its impact on the oceanic freshwater cycle. *Journal of Geophysical Research: Oceans*, *119*, 1271–1305. <https://doi.org/10.1002/2013JC008999>
- Lévy, M., Estublier, A., & Madec, G. (2001). Choice of an advection scheme for biogeochemical models. *Geophysical Research Letters*, *28*(19), 3725–3728.
- Lique, C., Treguier, A. M., Blanke, B., & Grima, N. (2010). On the origins of water masses exported along both sides of Greenland: A Lagrangian model analysis. *Journal of Geophysical Research*, *115*, C05019. <https://doi.org/10.1029/2009JC005316>
- Madec, G., & Imbard, M. (1996). A global ocean mesh to overcome the North Pole singularity. *Climate Dynamics*, *12*(6), 381–388.
- Madec, G., & the NEMO team (2008). *NEMO ocean engine*. France, No 27, ISSN No 1288–1619: Note du Pôle de modélisation, Institut Pierre-Simon Laplace (IPSL).
- Manucharyan, G. E., & Spall, M. A. (2016). Wind-driven freshwater buildup and release in the Beaufort Gyre constrained by mesoscale eddies. *Geophysical Research Letters*, *43*, 273–282. <https://doi.org/10.1002/2015GL065957>
- Manucharyan, G. E., Spall, M. A., & Thompson, A. F. (2016). A theory of the wind-driven Beaufort Gyre variability. *Journal of Physical Oceanography*, *46*(11), 3263–3278. <https://doi.org/10.1175/JPO-D-16-0091.1>
- Masina, S., Storto, A., Ferry, N., Valdivieso, M., Haines, K., Balmaseda, M., et al. (2017). An ensemble of eddy-permitting global ocean reanalyses from the MyOcean project. *Climate Dynamics*, *49*(3), 813–841.
- Meneghello, G., Marshall, J., Cole, S. T., & Timmermans, M.-L. (2017). Observational inferences of lateral eddy diffusivity in the halocline of the beaufort gyre. *Geophysical Research Letters*, *44*, 12–331. <https://doi.org/10.1002/2017GL075126>
- Mesinger, F., & Arakawa, A. (1976). Numerical methods used in atmospheric models, *GARP technical report 17*. 1, 17.
- Mizobata, K., Watanabe, E., & Kimura, N. (2016). Wintertime variability of the Beaufort gyre in the Arctic Ocean derived from CryoSat-2/SIRAL observations. *Journal of Geophysical Research: Oceans*, *121*, 1685–1699. <https://doi.org/10.1002/2015JC011218>
- Morison, J., Kwok, R., Peralta-Ferriz, C., Alkire, M., Rigor, I., Andersen, R., & Steele, M. (2012). Changing Arctic Ocean freshwater pathways. *Nature*, *481*(7379), 66–70. <https://doi.org/10.1038/nature10705>
- Nurser, A. J. G., & Bacon, S. (2014). The Rossby radius in the Arctic Ocean. *Ocean Science*, *10*(6), 967–975. <https://doi.org/10.5194/os-10-967-2014>
- Pickart, R. S., Moore, G. W. K., Mao, C., Bahr, F., Nobre, C., & Weingartner, T. J. (2016). Circulation of winter water on the Chukchi shelf in early Summer. *Deep Sea Research Part II: Topical Studies in Oceanography*, *130*, 56–75. <https://doi.org/10.1016/j.dsr2.2016.05.001>
- Proshutinsky, A. Y., Krishfield, R., Timmermans, M. L., Toole, J., Carmack, E. C., McLaughlin, F. A., et al. (2009). Beaufort Gyre freshwater reservoir: State and variability from observations. *Journal of Geophysical Research*, *114*, C00A10. <https://doi.org/10.1029/2008JC005104>
- Rabe, B., Karcher, M., Kauker, F., Schauer, U., Toole, J. M., Krishfield, R. A., et al. (2014). Arctic Ocean basin liquid freshwater storage trend 1992–2012. *Geophysical Research Letters*, *41*, 961–968. <https://doi.org/10.1002/2013GL058121>
- Rabe, B., Karcher, M., Schauer, U., Toole, J. M., Krishfield, R. A., Pisarev, S., et al. (2011). An assessment of Arctic Ocean freshwater content changes from the 1990s to the 2006–2008 period. *Deep Sea Research Part I: Oceanographic Research*, *58*, 173–185.
- Regan, H. C., Lique, C., & Armitage, Thomas W. K. (2019). The Beaufort Gyre extent, shape, and location between 2003 and 2014 from satellite observations. *Journal of Geophysical Research: Oceans*, *124*, 844–862. <https://doi.org/10.1029/2018JC014379>
- Roy, F., Chevallier, M., Smith, G. C., Dupont, F., Garric, G., Lemieux, J.-F., et al. (2015). Arctic sea ice and freshwater sensitivity to the treatment of the atmosphere-ice-ocean surface layer. *Journal of Geophysical Research: Oceans*, *120*, 4392–4417. <https://doi.org/10.1002/2014JC010677>
- Serreze, M. C., Barrett, A. P., Slater, A. G., Woodgate, R. A., Aagaard, K., Lammers, R. B., et al. (2006). The large-scale freshwater cycle of the Arctic. *Journal of Geophysical Research*, *111*, C11010. <https://doi.org/10.1029/2005JC003424>
- Serreze, M. C., Crawford, A. D., Stroeve, J. C., Barrett, A. P., & Woodgate, R. A. (2016). Variability, trends, and predictability of seasonal sea ice retreat and advance in the Chukchi Sea. *Journal of Geophysical Research: Oceans*, *121*, 7308–7325. <https://doi.org/10.1002/2016JC011977>
- Shimada, K., Kamoshida, T., Itoh, M., Nishino, S., Carmack, E., McLaughlin, F., et al. (2006). Pacific Ocean inflow: Influence on catastrophic reduction of sea ice cover in the Arctic Ocean. *Geophysical Research Letters*, *33*, L08605. <https://doi.org/10.1029/2005GL025624>
- Smith, G. C., Roy, F., Mann, P., Dupont, F., Brasnett, B., Lemieux, J.-F., et al. (2014). A new atmospheric dataset for forcing ice-ocean models: Evaluation of reforecasts using the Canadian global deterministic prediction system. *Quarterly Journal of the Royal Meteorological Society*, *140*(680), 881–894.
- Spall, M. A., Pickart, R. S., Fratantoni, P. S., & Plueddemann, A. J. (2008). Western Arctic shelfbreak eddies: Formation and transport. *Journal of Physical Oceanography*, *38*(8), 1644–1668.
- Spall, M. A., Pickart, R. S., Li, M., Itoh, M., Lin, P., Kikuchi, T., & Qi, Y. (2018). Transport of Pacific water into the Canada Basin and the formation of the Chukchi Slope Current. *Journal of Geophysical Research: Oceans*, *123*, 7453–7471. <https://doi.org/10.1029/2018JC013825>
- Steele, M., Morison, J., Ermold, W., Rigor, I., Ortmeyer, M., & Shimada, K. (2004). Circulation of summer Pacific halocline water in the Arctic Ocean. *Journal of Geophysical Research*, *109*, C02027. <https://doi.org/10.1029/2003JC002009>
- Timmermans, M.-L., Marshall, J., Proshutinsky, A., & Scott, J. (2017). Seasonally derived components of the Canada Basin halocline. *Geophysical Research Letters*, *44*, 5008–5015. <https://doi.org/10.1002/2017GL073042>
- Tsubouchi, T., Bacon, S., Naveira-Garabato, A. C., Sanders, R., McLaughlin, F. A., Petrie, B., et al. (2013). Export of nutrients from the Arctic Ocean. *Journal of Geophysical Research: Oceans*, *118*, 1625–1644. <https://doi.org/10.1002/jgrc.20063>
- Wang, Q., Wekerle, C., Danilov, S., Koldunov, N., Sidorenko, D., Sein, D., et al. (2018). Arctic sea ice decline significantly contributed to the unprecedented liquid freshwater accumulation in the Beaufort Gyre of the Arctic Ocean. *Geophysical Research Letters*, *45*, 4956–4964. <https://doi.org/10.1029/2018GL077901>
- Watanabe, E. (2011). Beaufort shelf break eddies and shelf-basin exchange of Pacific summer water in the western Arctic Ocean detected by satellite and modeling analyses. *Journal of Geophysical Research*, *116*, C08034. <https://doi.org/10.1029/2010JC006259>
- Weingartner, T. J., Potter, R. A., Stoudt, C. A., Dobbins, E. L., Statscewich, H., Winsor, P. R., et al. (2017). Transport and thermohaline variability in Barrow Canyon on the Northeastern Chukchi Sea Shelf. *Journal of Geophysical Research: Oceans*, *122*, 3565–3585. <https://doi.org/10.1002/2016JC012636>
- Woodgate, R. A. (2018). Increases in the Pacific inflow to the Arctic from 1990 to 2015, and insights into seasonal trends and driving mechanisms from year-round Bering Strait mooring data. *Progress in Oceanography*, *160*, 124–154. <https://doi.org/10.1016/j.pocan.2017.12.007>
- Woodgate, R. A., & Aagaard, K. (2005). Revising the Bering Strait freshwater flux into the Arctic Ocean. *Geophysical Research Letters*, *32*, L02602. <https://doi.org/10.1029/2004GL021747>

- Woodgate, R. A., Aagaard, K., & Weingartner, T. J. (2005). Monthly temperature, salinity, and transport variability of the Bering Strait through flow. *Geophysical Research Letters*, *32*, L04601. <https://doi.org/10.1029/2004GL021880>
- Woodgate, R. A., Aagaard, K., & Weingartner, T. J. (2006). Interannual changes in the Bering Strait fluxes of volume, heat and freshwater between 1991 and 2004. *Geophysical Research Letters*, *33*, L15609. <https://doi.org/https://doi.org/10.1029/2006GL026931>
- Woodgate, R. A., Weingartner, T. J., & Lindsay, R. (2010). The 2007 Bering Strait oceanic heat flux and anomalous Arctic sea-ice retreat. *Geophysical Research Letters*, *37*, L01602. <https://doi.org/10.1029/2009GL041621>
- Yamamoto-Kawai, M., McLaughlin, F. A., Carmack, E. C., Nishino, S., & Shimada, K. (2008). Freshwater budget of the Canada Basin, Arctic Ocean, from salinity,  $\delta^{18}\text{O}$ , and nutrients. *Journal of Geophysical Research*, *113*, C01007. <https://doi.org/10.1029/2006JC003858>
- Yang, J. (2006). The seasonal variability of the Arctic Ocean Ekman transport and its role in the mixed layer heat and salt fluxes. *Journal of Climate*, *19*(20), 5366–5387.
- Yang, J., Proshutinsky, A., & Lin, X. (2016). Dynamics of an idealized Beaufort Gyre: 1. The effect of a small beta and lack of western boundaries. *Journal of Geophysical Research: Oceans*, *121*, 1249–1261. <https://doi.org/10.1002/2015JC011296>
- Zhang, J., & Steele, M. (2007). Effect of vertical mixing on the Atlantic Water layer circulation in the Arctic Ocean. *Journal of Geophysical Research*, *112*, C04S04. <https://doi.org/10.1029/2006JC003732>
- Zhang, J., Steele, M., Runciman, K., Dewey, S., Morison, J., Lee, C., et al. (2016). The Beaufort Gyre intensification and stabilization: A model-observation synthesis. *Journal of Geophysical Research Oceans: Oceans*, *121*, 7933–7952. <https://doi.org/10.1002/2016JC012196>
- Zhao, M., Timmermans, M., Cole, S., Krishfield, R., & Toole, J. (2016). Evolution of the eddy field in the Arctic Ocean's Canada Basin, 2005–2015. *Geophysical Research Letters*, *43*, 8106–8114. <https://doi.org/10.1002/2016GL069671>